

# Transient Stability Analysis of Power Systems with Multiple Grid-forming Voltage Source Converters Using Reduced-order Modeling Method

Lei Chen, Tianhao Wen, Yuqing Lin, Yang Liu, *Member, IEEE*, Yingjie Qin, Qing-Hua Wu, *Life Fellow, IEEE*

**Abstract**—The traditional power system dominated by synchronous generators is gradually evolving into a modern power system featured by high-penetrated renewable energy. As a key technology for high-penetrated renewable energy, the grid-forming voltage source converter (GFM-VSC) has received increasing attention. However, the large-disturbance stability analysis of power systems with multiple GFM-VSCs is still a challenging problem due to various limitations of existing methods, including huge computational burden and difficulty in considering network losses. This paper is intended to address these issues from the perspective of reduced-order modeling and domain of attraction (DA) estimation. The innovations involve three aspects. First, the reduced-order modeling method for power systems with multiple GFM-VSCs is proposed using the standard dual-time-scale model in singular perturbation theory. Second, an expanding annular domain (EAD) algorithm is developed to estimate the DA with an entire boundary to analyze the large-disturbance stability of power systems. Third, the conditions of using the reduced-order modeling method based on singular perturbation theory have been clarified. The validity of the reduced-order modeling method is illustrated on a modified 39-bus system with 10 GFM-VSCs.

**Index Terms**—Transient stability, voltage source converter (VSC), grid-forming (GFM), domain of attraction (DA), reduced-order modeling, singular perturbation theory, expanding annular domain (EAD).

## I. INTRODUCTION

VOLTAGE source converters (VSCs) are widely integrated into modern power systems as the grid interfaces of renewable energy sources [1]–[3]. The VSC can be considered as a voltage source whose phase and amplitude are con-

trolled by the control strategy inside, which mainly includes grid-forming VSC (GFM-VSC) and grid-following VSC (GFL-VSC) [4]. The GFL-VSC is designed to track the angle and frequency of power grid via a phase-locked loop (PLL), but it could become unstable when the grid impedance is very high. Compared with GFL-VSC, the GFM-VSC has better performance on the virtual inertia provision [5] and frequency response [6], making it more applicable to weak power grids [7], [8]. Therefore, the GFM-VSC is a promising technique for power systems with high-penetrated renewable energy.

The stability of power system with GFM-VSC can be distinguished as small-disturbance stability [9]–[13] and large-disturbance stability [4], [14], [15]. The small-disturbance stability is analyzed by linearizing the system around a given operating point, which cannot capture the nonlinear characteristics of GFM-VSC. According to [16], the large-disturbance stability can be divided into synchronous stability (transient stability) and large-disturbance voltage stability. This paper focuses on the former that is defined as the ability to maintain synchronism with the grid when the VSC suffers large disturbances.

Different control strategies of GFM-VSC have different external characteristics for the power grid. The control strategies of GFM-VSC are composed of virtual oscillator control, droop control, and virtual synchronous generator (VSG) control [9], [17]. Without loss of generality, the VSG is considered as a representative of grid-forming (GFM) control in this study.

Generally, methods for analyzing the transient stability of power system with GFM-VSC are classified into time-domain simulation [18] and direct methods [19]. As the most widely adopted method, the time-domain simulation can consider detailed models and give accurate results via numerical integration of post-fault dynamics. Nonetheless, the time-domain simulation is too time-consuming and cannot provide stability margin. It also cannot reveal physical insights into the stability mechanism of power system with GFM-VSC. To reduce the computational cost and provide the stability margin, the direct methods for transient stability analysis of power system with GFM-VSC have been explored in recent decades. Domain of attraction (DA) is a core concept in direct methods. For a given asymptotically stable equilibrium

Manuscript received: October 28, 2024; revised: December 28, 2024; accepted: July 8, 2025. Date of CrossCheck: July 8, 2025. Date of online publication: August 25, 2025.

This work was supported by the Department of Science and Technology of Guangdong Province (No. 2023A1515240019).

This article is distributed under the terms of the Creative Commons Attribution 4.0 International License (<http://creativecommons.org/licenses/by/4.0/>).

L. Chen is with the Electric Power Research Institute, China Southern Power Grid, Guangzhou, China (e-mail: chenlei96918@163.com).

T. Wen (corresponding author), Y. Lin, Y. Liu, and Q.-H. Wu are with the School of Electric Power Engineering, South China University of Technology, Guangzhou, China (e-mail: epwentianhao@scut.edu.cn; lyqscut415@163.com; epyangliu@scut.edu.cn; wuqh@scut.edu.cn).

Y. Qin is with the Power Dispatching and Control Center, Guangdong Power Grid Corporation, Guangzhou, China (e-mail: qinyingjie@gpdc.gd.csg.cn).

DOI: 10.35833/MPCE.2024.001166



point (ASEP), the DA is a set of initial states, and all trajectories starting from this domain will converge to the equilibrium point. By estimating the DA, one can directly calculate the stability margin of systems with respect to a given initial state [20]. It can also avoid the time-consuming integration of the post-fault system dynamics and provide guidances for the design of stabilization controllers. According to [19], the exact DA is the set of stable manifolds of all unstable equilibrium points (UEPs) on the stability boundary. However, the calculation of all UEPs and their stable manifolds is extremely complicated and often inaccurate, especially for large-scale power systems. For these reasons, almost all relevant studies have focused on DA estimation using the level sets of Lyapunov or energy functions. This paper will also analyze the transient stability of power systems with multiple GFM-VSCs from this perspective.

In general, direct methods can be divided into equal area criterion (EAC) method [21], phase portrait method [14], [22], energy function method [4], [23], Hamiltonian-based energy function method [24], and Lyapunov function method [25]. Indeed, these studies provide useful insights into transient stability analysis of power system with GFM-VSC from different aspects. Nevertheless, the EAC and phase portrait methods are only suitable for transient stability analysis of single grid-connected GFM-VSC system. There is no analytical energy function or Hamiltonian-based energy function for lossy systems, and numerical energy function method may result in stability misjudgment. The primary difficulty of Lyapunov function method is the lack of a systematic method to construct the Lyapunov function. Recent studies on the sum of squares (SOS) program provide an effective method to deal with this issue [26], [27]. In terms of transient stability analysis of converter-dominant power systems, [28]-[30] use the SOS programming to estimate the DA of single-VSC infinite-bus systems, but these studies only involve GFL-VSC and the analyzed systems are too simple, which cannot describe the detailed dynamics of power systems with multiple GFM-VSCs. The expanding interior algorithm [31], [32] and expanding annular domain (EAD) algorithm [33] are the pioneering explorations of the DA estimation of synchronous generator (SG)-dominant power systems using SOS program, which provides promising tools for transient stability analysis of power systems with multiple VSCs. However, the computational burden of SOS-based methods is positively correlated with system scale, so it is difficult to directly apply SOS-based methods to large-scale systems. If the model order can be reduced, the SOS-based methods will be more applicable for transient stability analysis of large-scale systems with multiple VSCs.

With regard to model order reduction, [34] and [35] report the reduced-order modeling of power systems with multiple VSCs, but both only involve multiple GFL-VSCs and the structure of analyzed system is too idealistic, i.e., multiple converters are connected to the same point of common coupling (PCC) with a parallel configuration. This reduced-order modeling method has a limited applicability and cannot be applied to power systems where multiple converters are connected to different PCCs. Further exploration is still required.

In summary, despite a lot of investigations on the transient stability analysis of idealistic power systems, seldom has analyzed the transient stability of complex power systems with multiple GFM-VSCs. The recent work [23] has conducted relevant studies, but it provides the optimistic estimated results using numerical energy function method. A more accurate and applicable method is still needed to analyze the transient stability of power systems with multiple GFM-VSCs. The SOS-based methods are promising for addressing this issue, and the reasons are fourfold. First, the SOS-based methods can construct Lyapunov function and compute the maximum critical value for lossy systems systematically, and the results obtained are more accurate than those produced by numerical energy function method. Second, the DA estimation using SOS-based methods is applicable for transient stability analysis of power systems with multiple SGs, which has been illustrated in our previous study [33]. Third, the computational efforts of SOS-based methods can be reduced by the reduced-order modeling method. Fourth, the SOS-based methods can estimate the DA with an entire boundary that contributes to addressing a group of contingencies. Main contributions are summarized as follows.

- 1) By using the standard dual-time-scale model in singular perturbation theory, the reduced-order modeling method of power systems with multiple GFM-VSCs, which are denoted as multi-VSC power systems for simplicity, is first proposed, which reduces the order of system model and computational burden of DA estimation significantly.
- 2) An efficient EAD algorithm to estimate the DA with an entire boundary for multi-VSC power systems is developed. This is more accurate compared with the existing global DA estimation methods.
- 3) The influence of parameters on the transient stability is analyzed quantitatively, which helps clarify the conditions of using the reduced-order modeling method based on singular perturbation theory.

Till now, the reduced-order modeling method combined with the concept of SOS program has not been applied to the DA estimation of multi-VSC power systems.

The rest of this paper is organized as follows. In Section II, the structure and equivalent model of a VSG-controlled GFM-VSC system are introduced. In Section III, based on the full-order model of multi-VSC power system, the reduced-order model is derived using singular perturbation theory, and the reduced-order model is transformed into a polynomial one via the polynomial transformation. Section IV develops the EAD algorithm to estimate the DA of multi-VSC power systems. The effectiveness of our work is illustrated on a modified 39-bus system with 10 GFM-VSCs in Section V. Finally, conclusions are presented in Section VI.

**Notation** For  $\mathbf{x} \in \mathbb{R}^M$ ,  $\mathbb{P}_M[\mathbf{x}]$  and  $\Sigma_M[\mathbf{x}]$  are the sets of polynomials and SOS polynomials, respectively;  $\mathbb{P}_M^N$  is the set of  $N$ -dimensional vector of polynomials with  $M$  variables;  $\deg(p_1, p_2, \dots, p_n)$  is the maximum degree of all polynomials in the set  $\{p_1, p_2, \dots, p_n\}$ . For a map  $\mathbf{A}: \mathbb{R}^M \rightarrow \mathbb{R}^N$ ,  $\mathbf{A} \in \mathcal{C}^k(\mathbb{R}^M; \mathbb{R}^N)$  ( $k \geq 1$ ) means that  $\mathbf{A}$  has the  $k^{\text{th}}$ -order continuous partial derivatives in  $\mathbb{R}^M$ .



Based on the above analysis, the dynamic equations of VSG-controlled GFM-VSC in Figs. 1 and 2 are:

$$\begin{cases} \dot{\theta} = \omega \\ J\dot{\omega} = P_{\text{ref}} - P_e - K_d\omega \end{cases} \quad (1)$$

### III. REDUCED-ORDER MODEL USING SINGULAR PERTURBATION THEORY

This paper is intended to estimate the DA of multi-VSC power systems. To this end, we construct the full-order model of multi-VSC power systems at first. Then, the standard dual-time-scale model in singular perturbation theory [40] is used to derive the reduced-order model of multi-VSC power systems. It is worth noting that singular perturbation theory is suitable for large-disturbance stability analysis [19], [40], [41].

#### A. Full-order Model of Multi-VSC Power Systems

According to (1), we consider a multi-VSC power system consisting of  $n$  GFM-VSCs and  $m$  constant impedance loads (CILs), as depicted in Fig. 4, where  $V_i$  is the voltage magnitude of GFM-VSC  $i$ ; and  $y_i$  is the admittance between node  $i$  and node  $n+i$ .

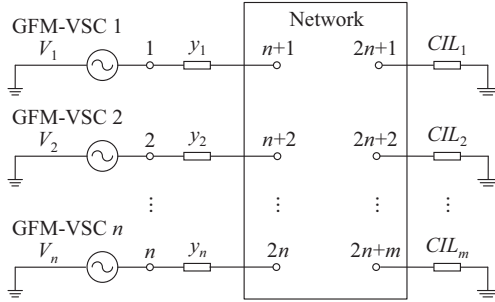


Fig. 4. Multi-VSC power system with  $n$  GFM-VSCs and  $m$  CILs.

By incorporating all CILs into the network admittance matrix and eliminating all the terminal buses of the network, we can obtain its internal model that is similar to the internal model of systems containing SGs and CILs [42]. Then, GFM-VSC  $n$  is selected as the reference machine, and the dynamics of this system are described by:

$$\begin{cases} \dot{\theta}_{1n} = \omega_1 - \omega_n \\ \vdots \\ \dot{\theta}_{(n-1)n} = \omega_{n-1} - \omega_n \\ \dot{\omega}_1 = (P_{\text{ref}1} - P_{e1} - K_{d1}\omega_1)/J_1 \\ \vdots \\ \dot{\omega}_n = (P_{\text{ref}n} - P_{en} - K_{dn}\omega_n)/J_n \end{cases} \quad (2)$$

where  $P_{ei} = \sum_{j=1}^n V_i V_j (G_{ij} \cos(\theta_{in} - \theta_{jn}) + B_{ij} \sin(\theta_{in} - \theta_{jn}))$ ,  $i = 1, 2, \dots, n$ ,  $\theta_{in}$  and  $\theta_{jn}$  are the virtual power angles of GFM-VSC  $i$  and GFM-VSC  $j$  with respect to GFM-VSC  $n$ , respectively,  $V_i = V_{di}$ , and  $G_{ij}$  and  $B_{ij}$  are the conductance and susceptance between GFM-VSC  $i$  and GFM-VSC  $j$ , respectively.

To facilitate the employment of the standard dual-time-scale model in singular perturbation theory [40], system (2)

can also be expressed as:

$$\begin{cases} \dot{\theta}_{1n} = \omega_1 - \omega_n \\ \vdots \\ \dot{\theta}_{(n-1)n} = \omega_{n-1} - \omega_n \\ \frac{1}{\omega_b} \dot{\omega}_1 = \frac{1}{2H_1} (P_{\text{ref}1} - P_{e1} - K_{d1}\omega_1) \\ \vdots \\ \frac{1}{\omega_b} \dot{\omega}_n = \frac{1}{2H_n} (P_{\text{ref}n} - P_{en} - K_{dn}\omega_n) \end{cases} \quad (3)$$

where  $H_i = J_i \omega_b / 2$  is the equivalent inertial coefficient of GFM-VSC  $i$ .

Considering the similarity between model (3) and standard dual-time-scale model, we will utilize several properties of the latter to derive the reduced-order model of system (3).

#### B. Reduced-order Model of Multi-VSC Power Systems

##### 1) Derivation of Boundary-layer Model

The standard dual-time-scale model [40] is expressed as:

$$\begin{cases} \frac{dx}{dt} = f(x, y) \\ \epsilon \frac{dy}{dt} = g(x, y) \end{cases} \quad (4)$$

where  $x \in \mathbb{R}^n$ ;  $y \in \mathbb{R}^m$ ;  $\epsilon$  is a small positive number; and  $f: \mathbb{R}^n \times \mathbb{R}^m \rightarrow \mathbb{R}^n$  and  $g: \mathbb{R}^n \times \mathbb{R}^m \rightarrow \mathbb{R}^m$  are the polynomial vector fields,  $f \in C^2(\mathbb{R}^{n+m}; \mathbb{R}^n)$ , and  $g \in C^2(\mathbb{R}^{n+m}; \mathbb{R}^m)$ .

Define  $x = [\theta_{1n}, \theta_{2n}, \dots, \theta_{(n-1)n}]^T$  and  $y = [\omega_1, \omega_2, \dots, \omega_n]^T$ , and then model (3) can be expressed in the form of model (4).

Let  $\tau\epsilon = t$ , and system (4) can be transformed into:

$$\begin{cases} \frac{dx}{d\tau} = \mathcal{F}(x, y) \\ \frac{dy}{d\tau} = \mathcal{G}(x, y) \end{cases} \quad (5)$$

When  $\epsilon = 0$ , system (5) becomes:

$$\begin{cases} \frac{dx}{d\tau} = \mathbf{0} \\ \frac{dy}{d\tau} = \mathcal{G}(x, y) \end{cases} \quad (6)$$

According to [40], system (6) is the boundary-layer system of (4).

##### 2) Analysis of Boundary-layer Model

The state vector  $x$  can be regarded as constant in system (6) since  $dx/d\tau = \mathbf{0}$ . Based on systems (3) and (6), combined with  $\tau\epsilon = t$ , we have:

$$\frac{dy_i}{d\tau} = \frac{d\omega_i}{d\tau} = \epsilon \frac{d\omega_i}{dt} \approx \frac{1}{\omega_b} \frac{d\omega_i}{dt} = \frac{P_{\text{ref}i} - P_{ei}}{2H_i} - \frac{K_{di}\omega_i}{2H_i} \quad (7)$$

Based on the above derivation, we outline the following conditions of boundary-layer system (6).

- 1)  $x$  is regarded as a constant vector in (6).
  - 2)  $x$  only consists of relative angle  $\theta_{in}$ .
  - 3)  $G_{ij}$ ,  $B_{ij}$ ,  $P_{\text{ref}i}$ ,  $V_i$ , and  $H_i$  are constant, so  $(P_{\text{ref}i} - P_{ei})/(2H_i)$  is only a function of  $\theta_{in}$ .
- As a result,  $(P_{\text{ref}i} - P_{ei})/(2H_i)$  is constant, so the stability

of (7) only depends on negative linear term  $-K_{di}\omega_i/(2H_i)$ . In addition, the negative linear term  $-K_{di}\omega_i/(2H_i)$  is globally asymptotically stable according to Theorem 4.5 in [40]. Hence, the fast dynamics (rotor angular frequency) denoted by (7) are globally asymptotically stable and can be ignored in the transient stability analysis of the original system (4).

### 3) Derivation of Reduced-order Model

The neglect of fast dynamics in the transient stability analysis of original system (4) means that  $\epsilon dy/dt = \mathbf{g}(\mathbf{x}, \mathbf{y}) = \mathbf{0}$  since  $\epsilon = 0$ , but  $dy/dt \neq \mathbf{0}$ . Thus, system (4) can be converted into the following general reduced-order model:

$$\begin{cases} \frac{d\mathbf{x}}{dt} = \mathbf{f}(\mathbf{x}, \mathbf{y}) \\ \mathbf{0} = \mathbf{g}(\mathbf{x}, \mathbf{y}) \end{cases} \quad (8)$$

In essence, the dynamics of  $\mathbf{y}$  in general reduced-order model (8) are totally controlled by the dynamics of  $\mathbf{x}$ , which further indicates that  $dy/dt \neq \mathbf{0}$ .

Equivalently, system (3) can be converted into:

$$\begin{cases} \dot{\theta}_{1n} = \omega_1 - \omega_n \\ \vdots \\ \dot{\theta}_{(n-1)n} = \omega_{n-1} - \omega_n \\ 0 = \frac{1}{2H_1} (P_{ref1} - P_{e1} - K_{d1}\omega_1) \\ \vdots \\ 0 = \frac{1}{2H_n} (P_{refn} - P_{en} - K_{dn}\omega_n) \end{cases} \quad (9)$$

From system (9), we can obtain:

$$\frac{P_{refi} - P_{ei}}{2H_i} - \frac{K_{di}\omega_i}{2H_i} = 0 \Rightarrow \omega_i = \frac{P_{refi} - P_{ei}}{K_{di}} \quad (10)$$

Substituting (10) into (9), the following reduced-order model is obtained:

$$\begin{cases} \dot{\theta}_{1n} = \frac{P_{ref1} - P_{e1}}{K_{d1}} - \frac{P_{refn} - P_{en}}{K_{dn}} \\ \vdots \\ \dot{\theta}_{(n-1)n} = \frac{P_{ref(n-1)} - P_{e(n-1)}}{K_{d(n-1)}} - \frac{P_{refn} - P_{en}}{K_{dn}} \end{cases} \quad (11)$$

The general derivation of reduced-order model can be found in formulas (11.1)-(11.5) in [40].

**Remark 1** The reduced-order model (11) has neglected the dynamics of rotor angular frequency since the dynamics of rotor angular frequency are globally asymptotically stable, reducing the dimension of state vector  $\mathbf{x}$  from  $2n-1$  to  $n-1$ . Obviously, the state vector of reduced-order model (11) is  $\mathbf{x}_r = [\theta_{1n}, \theta_{2n}, \dots, \theta_{(n-1)n}]^T$ , while that of full-order model (3) is denoted by  $\mathbf{x}_f = [\theta_{1n}, \theta_{2n}, \dots, \theta_{(n-1)n}, \omega_1, \omega_2, \dots, \omega_n]^T$ .

**Remark 2** In Section II-B, the dynamics of voltage, current, and reactive power control loops are neglected to obtain state equations of GFM-VSC that are similar to those of SG. Section II-C derives the reduced-order model of multi-VSC power systems to further reduce the model order by ignoring the dynamics of rotor angular frequency. The former is to facilitate the construction of state equations of multi-

VSC power systems and obtain its internal model. The latter aims to reduce the dimension of state vector, resulting in a dramatic reduction in the computational burden of DA estimation of multi-VSC power systems with larger sizes.

**Remark 3** The reduced-order model (8) is entirely equivalent to full-order model (4) only when  $\epsilon = 0$ . To reduce the gap between the full-order model and reduced-order model of multi-VSC power systems, the coefficients on the right side of formula (3) should be far larger than the one on the left side, i.e.,  $1/(2H_i) \gg 1/\omega_b$  and  $K_{di}/(2H_i) \gg 1/\omega_b$ . Note that the above reduced-order modeling method is not applicable to SG-dominant power system due to its huge gap between the full-order model and reduced-order model. Detailed comparisons are provided in Section V.

The power-frequency droop-controlled GFM-VSC in [17] has similar external behaviors to the first-order frequency-dependent load, the DA estimation of which can also be addressed by our algorithm in Section IV. In this case, the reduced-order modeling is not required.

### C. Coordinate Transformation

Formula (11) is not a polynomial system due to the existence of sine and cosine terms in  $P_{ei}$ , while the SOS-based methods are only suitable for estimating the DA of polynomial systems. Hence, we shift the ASEP of (11) to the origin for simplicity and transform this shifted system into a polynomial system via the polynomial transformation  $\mathbf{z} = \mathbf{h}(\mathbf{x})$ , where  $\mathbf{h}: \mathbb{R}^{n-1} \rightarrow \mathbb{R}^{2n-2}$  is the function making (12) hold.

$$\begin{cases} z_{2i-1} = \sin x_i \\ z_{2i} = 1 - \cos x_i \end{cases} \quad i = 1, 2, \dots, n-1 \quad (12)$$

The transformed polynomial system can be expressed as:

$$\begin{cases} \dot{\mathbf{z}} = \mathbf{F}(\mathbf{z}) \\ \mathbf{G}(\mathbf{z}) = \mathbf{0} \end{cases} \quad (13)$$

where  $\mathbf{z} \in \mathbb{R}^M$  ( $M = 2n-2$ ) is the state vector of the transformed polynomial system, denoted as  $\mathbf{z} = [z_1, z_2, \dots, z_{2n-3}, z_{2n-2}]$ ; and  $\mathbf{F}: \mathbb{R}^M \rightarrow \mathbb{R}^M$  and  $\mathbf{G}: \mathbb{R}^M \rightarrow \mathbb{R}^N$  ( $N = n-1$ ) are the polynomial functions.

Specifically, system (13) can be represented as:

$$\begin{cases} \dot{z}_1 = (1 - z_2) \left( \frac{P_{ref1} - P_{e1}(\mathbf{z})}{K_{d1}} - \frac{P_{refn} - P_{en}(\mathbf{z})}{K_{dn}} \right) \\ \dot{z}_2 = z_1 \left( \frac{P_{ref1} - P_{e1}(\mathbf{z})}{K_{d1}} - \frac{P_{refn} - P_{en}(\mathbf{z})}{K_{dn}} \right) \\ \vdots \\ \dot{z}_{2n-3} = (1 - z_{2n-2}) \left( \frac{P_{ref(n-1)} - P_{e(n-1)}(\mathbf{z})}{K_{d(n-1)}} - \frac{P_{refn} - P_{en}(\mathbf{z})}{K_{dn}} \right) \\ \dot{z}_{2n-2} = z_{2n-3} \left( \frac{P_{ref(n-1)} - P_{e(n-1)}(\mathbf{z})}{K_{d(n-1)}} - \frac{P_{refn} - P_{en}(\mathbf{z})}{K_{dn}} \right) \end{cases} \quad (14)$$

$$\begin{cases} G_1(\mathbf{z}) = z_1^2 + z_2^2 - 2z_2 = 0 \\ G_2(\mathbf{z}) = z_3^2 + z_4^2 - 2z_4 = 0 \\ \vdots \\ G_{n-1}(\mathbf{z}) = z_{2n-3}^2 + z_{2n-2}^2 - 2z_{2n-2} = 0 \end{cases} \quad (15)$$

$$P_{ei}(\mathbf{z}) = \sum_{j=1}^{n-1} V_i V_j \{G_{ij}[(1-z_{2i})(1-z_{2j}) + z_{2i-1}z_{2j-1}] + B_{ij}[z_{2i-1}(1-z_{2j}) - (1-z_{2i})z_{2j-1}]\} + V_i V_n [G_{in}(1-z_{2n-2}) - B_{in}z_{2n-3}] \quad (16)$$

#### IV. DA ESTIMATION OF MULTI-VSC POWER SYSTEMS VIA EAD ALGORITHM

This paper is intended to analyze the transient stability of multi-VSC power systems from the perspective of DA estimation. For DA estimation, the EAD algorithm proposed in [33] is easier with only one iteration loop and two SOS programs (not including initialization). Besides, based on the modified Lyapunov stability theory [33], the EAD algorithm can obtain a larger estimated entire DA for lossy systems. Hence, we employ the EAD algorithm to estimate the DA of polynomial system (13) in this section.

##### A. SOS Program and S-procedure

For  $\mathbf{x} \in \mathbb{R}^M$ , a multivariate polynomial  $p(\mathbf{x})$  is an SOS [26] if there exist some polynomial functions  $p_1(\mathbf{x}), p_2(\mathbf{x}), \dots, p_N(\mathbf{x})$  satisfying:

$$p(\mathbf{x}) = \sum_{i=1}^N p_i^2(\mathbf{x}) \quad (17)$$

Clearly, being an SOS means that  $p(\mathbf{x}) \geq 0$  for all  $\mathbf{x} \in \mathbb{R}^M$ . The reverse, however, is not always true [31].

Before solving an SOS program, the S-procedure is utilized to obtain sufficient conditions for the set containment constraints as follows [43]: given  $g_0, g_1, \dots, g_K \in \mathbb{P}_M[\mathbf{x}]$ , if there exist  $\tilde{s}_1, \tilde{s}_2, \dots, \tilde{s}_K \in \Sigma_M[\mathbf{x}]$  making  $g_0 - \sum_{k=1}^K \tilde{s}_k g_k \in \Sigma_M[\mathbf{x}]$ , then  $\{\mathbf{x} \in \mathbb{R}^M | g_1(\mathbf{x}), g_2(\mathbf{x}), \dots, g_K(\mathbf{x}) \geq 0\} \subseteq \{\mathbf{x} \in \mathbb{R}^M | g_0(\mathbf{x}) \geq 0\}$ .

The SOS program is an optimization problem containing several SOS constraints that must be SOS polynomials. This kind of optimization problem can be transformed into a semi-definite programming (SDP) problem [44] that can be easily solved by off-the-shelf optimization techniques.

The solver MOSEK is an effective tool to perform this conversion for general SOS program problems and solve the transformed SDP problems. Thus, all SOS programs in this paper are addressed in MATLAB by the toolbox YALMIP [45] and solver MOSEK [46].

Besides, to understand set  $\mathbb{P}_{M^N}^N$  a 3-dimensional vector of polynomials with 4 variables denoted by  $\lambda_0 \in \mathbb{P}_4^3$  is defined as:

$$\lambda_0 = \begin{bmatrix} z_1^2 + z_2^2 - 2z_1 z_2 \\ z_3^2 + z_4^2 - z_1 z_2 - z_3 z_4 \\ z_1^2 + z_2^2 + z_3^2 + z_4^2 \end{bmatrix} \quad (18)$$

The EAD algorithm for DA estimation of polynomial system (13) contains two steps, which includes an initial DA estimation and its expansion, as shown in the following.

##### B. Initial DA Estimation

The DA of power systems can be estimated by a level set of Lyapunov function  $V(\mathbf{z})$  as:

$$D(V(\mathbf{z})) = \{\mathbf{z} \in \mathbb{R}^M | V(\mathbf{z}) \leq c, \mathbf{G}(\mathbf{z}) = \mathbf{0}, c > 0\} \quad (19)$$

where  $c$  is a critical value.

Meanwhile, a semi-algebraic region  $\hat{D}$  containing the origin is defined as:

$$\hat{D} = \{\mathbf{z} \in \mathbb{R}^M | p(\mathbf{z}) \leq \beta, \mathbf{G}(\mathbf{z}) = \mathbf{0}, \beta > 0\} \quad (20)$$

where  $p(\mathbf{z})$  is a positive definite polynomial; and  $\beta$  is a positive number.

According to the modified Lyapunov stability theory in [33], we search for a continuously differentiable function  $V_0(\mathbf{z}): \hat{D} \rightarrow \mathbb{R}$  with  $V_0(\mathbf{0}) = 0$  such that:

$$V_0(\mathbf{z}) > 0 \quad \forall \mathbf{z} \in \{\mathbf{z} \in \mathbb{R}^M | \mathbf{G}(\mathbf{z}) = \mathbf{0}\} \setminus \{0\} \quad (21a)$$

$$\dot{V}_0(\mathbf{z}) < 0 \quad \forall \mathbf{z} \in \{\mathbf{z} \in \mathbb{R}^M | \beta - p(\mathbf{z}) \geq 0, \mathbf{G}(\mathbf{z}) = \mathbf{0}\} \setminus \{0\} \quad (21b)$$

Then,  $\mathbf{z} = \mathbf{0}$  is an ASEP, and  $V_0(\mathbf{z})$  is a polynomial Lyapunov function of system (13).

Conditions in (21) can be converted into the set inclusion conditions, given as:

$$\{\mathbf{z} \in \mathbb{R}^M | \mathbf{G}(\mathbf{z}) = \mathbf{0}\} \setminus \{0\} \subseteq \{\mathbf{z} \in \mathbb{R}^M | V_0(\mathbf{z}) > 0\} \quad (22a)$$

$$\{\mathbf{z} \in \mathbb{R}^M | \beta - p(\mathbf{z}) \geq 0, \mathbf{G}(\mathbf{z}) = \mathbf{0}\} \setminus \{0\} \subseteq \{\mathbf{z} \in \mathbb{R}^M | \dot{V}_0(\mathbf{z}) < 0\} \quad (22b)$$

According to S-procedure, we can obtain the following SOS program to find a feasible solution  $V_{0a}(\mathbf{z})$ :

$$\text{SOSP0a: } \underset{V_{0a}(\mathbf{z}) \in \mathbb{P}_M[\mathbf{z}], V_{0a}(\mathbf{0}) = 0, \bar{s}_1 \in \Sigma_M[\mathbf{z}], \lambda_1, \lambda_2 \in \mathbb{P}_M^N[\mathbf{z}]}{\text{search}} V_{0a}(\mathbf{z}) \quad (23a)$$

s.t.

$$V_{0a}(\mathbf{z}) - \lambda_1^T \mathbf{G}(\mathbf{z}) - l_1 \in \Sigma_M[\mathbf{z}] \quad (23b)$$

$$-\dot{V}_{0a}(\mathbf{z}) - \bar{s}_1(\beta - p(\mathbf{z})) - \lambda_2^T \mathbf{G}(\mathbf{z}) - l_2 \in \Sigma_M[\mathbf{z}] \quad (23c)$$

where  $l_1 = \sigma_1 \sum_{i=1}^M z_i^d$  and  $l_2 = \sigma_2 \sum_{i=1}^M z_i^d$ ,  $\sigma_1$  and  $\sigma_2$  are the sufficiently small positive numbers, and  $d$  is an even number satisfying  $d \geq 2$ ;  $\bar{s}_j$  is an SOS polynomial with  $M$  variables; and  $\lambda_j$  is a  $N$ -dimensional vector of polynomials with  $M$  variables.

It is noted that different  $p(\mathbf{z})$  and  $\beta$  will give rise to different  $V_{0a}(\mathbf{z})$ . Generally, the region  $\hat{D}$  is selected to be small enough so that SOSP0a is feasible.

Since SOSP0a provides a feasible solution  $V_{0a}(\mathbf{z})$ , we will solve the following SOS program to obtain an initial estimated DA:

$$\text{SOSP0b: } \underset{\bar{s}_2 \in \Sigma_M[\mathbf{z}], \lambda_3 \in \mathbb{P}_M^N[\mathbf{z}]}{\max} c \quad (24a)$$

s.t.

$$-\dot{V}_{0a}(\mathbf{z}) - \bar{s}_2(c - V_{0a}(\mathbf{z})) - \lambda_3^T \mathbf{G}(\mathbf{z}) - l_2 \in \Sigma_M[\mathbf{z}] \quad (24b)$$

SOSP0b can be solved by using a bisection search on  $c$ . Then, denoting the solution of SOSP0b as  $c_0$ , an initial Lyapunov function and an initial DA are  $V_{(0)}(\mathbf{z}) = V_{0a}(\mathbf{z})/c_0$  and  $D_{(0)}(\mathbf{z}) = \{\mathbf{z} \in \mathbb{R}^M | V_{(0)}(\mathbf{z}) \leq 1, \mathbf{G}(\mathbf{z}) = \mathbf{0}\}$ , respectively.

##### C. Expansion of Estimated DA via EAD Algorithm

For polynomial system (13) and a known estimated DA  $D_{(k)}(\mathbf{z})$ , if there exists a continuously differentiable polynomial function  $V_{(k+1)}(\mathbf{z})$ , a positive number  $0 < \gamma \leq 1$ , and a bounded set  $D_{(k+1)}(\mathbf{z})$ , we have:

$$\begin{cases} V_{(k+1)}(\mathbf{0}) = 0 \\ V_{(k+1)}(\mathbf{z}) > 0 \quad \forall \mathbf{z} \in \{\mathbf{z} \in \mathbb{R}^M | \mathbf{G}(\mathbf{z}) = \mathbf{0}\} \setminus \{0\} \end{cases} \quad (25a)$$

$$\dot{V}_{(k+1)}(\mathbf{z}) < 0 \quad \forall \mathbf{z} \in \{\mathbf{z} \in \mathbb{R}^M | V_{(k+1)}(\mathbf{z}) \leq 1, V_{(k)}(\mathbf{z}) \geq \gamma, \mathbf{G}(\mathbf{z}) = \mathbf{0}\} \quad (25b)$$

$$D_{(k)}(\mathbf{z}) \subset D_{(k+1)}(\mathbf{z}) \quad (25c)$$

where  $k$  is the iteration index.

Based on S-procedure and SOS programming, conditions in (25) can be transformed into the following SOS program:

$$\text{SOSP1: } \underset{V_{(k+1)}(\mathbf{z}) \in \mathbb{P}_M[\mathbf{z}], V_{(k+1)}(\mathbf{0})=0, \bar{s}_3, \bar{s}_4, \bar{s}_5 \in \Sigma_M[\mathbf{z}], \lambda_4, \lambda_5, \lambda_6 \in \mathbb{P}_M^N[\mathbf{z}]}{\text{search}} V_{(k+1)}(\mathbf{z}) \quad (26a)$$

s.t.

$$V_{(k+1)}(\mathbf{z}) - \lambda_4^T \mathbf{G}(\mathbf{z}) - l \in \Sigma_M[\mathbf{z}] \quad (26b)$$

$$-\dot{V}_{(k+1)}(\mathbf{z}) - \bar{s}_3(1 - V_{(k+1)}(\mathbf{z})) - \bar{s}_4(V_{(k)}(\mathbf{z}) - \gamma) - \lambda_5^T \mathbf{G}(\mathbf{z}) - q_1 \in \Sigma_M[\mathbf{z}] \quad (26c)$$

$$-\bar{s}_5(1 + q_2 - V_{(k)}(\mathbf{z})) + (1 - V_{(k+1)}(\mathbf{z})) - \lambda_6^T \mathbf{G}(\mathbf{z}) \in \Sigma_M[\mathbf{z}] \quad (26d)$$

where  $q_1$  and  $q_2$  are the sufficiently small positive numbers;

and  $l = \sigma \sum_{i=1}^M z_i^d$ , and  $\sigma$  is a sufficiently small positive number.

Apparently, if the SOSP1 is feasible, then  $D_{(k+1)}(\mathbf{z})$  is a better estimated DA. Nevertheless, solving SOSP1 directly is NP-hard due to the bilinear term such as  $\bar{s}_3 V_{(k+1)}(\mathbf{z})$  in (26c).

To address this issue, the coordinate-wise iterative method in [47] and [48] is used to transform the above bilinear constraint into a linear one. Similar to SOSP2 in [33], we have:

$$\text{SOSP2: } \underset{\bar{s}_3, \bar{s}_4 \in \Sigma_M[\mathbf{z}], \lambda_5 \in \mathbb{P}_M^N[\mathbf{z}]}{\text{search}} \bar{s}_3 \quad (27a)$$

s.t.

$$-\dot{V}_{(k)}(\mathbf{z}) - \bar{s}_3(1 - V_{(k)}(\mathbf{z})) - \bar{s}_4(V_{(k)}(\mathbf{z}) - \gamma) - \lambda_5^T \mathbf{G}(\mathbf{z}) - q_1 \in \Sigma_M[\mathbf{z}] \quad (27b)$$

Then, we save the output of SOSP2  $\bar{s}_3$  as  $s_3$ . Combining SOSP2 with SOSP1, we have the following SOS program:

$$\text{SOSP3: } \underset{V_{(k+1)}(\mathbf{z}) \in \mathbb{P}_M[\mathbf{z}], V_{(k+1)}(\mathbf{0})=0, \bar{s}_4, \bar{s}_5, \bar{s}_6 \in \Sigma_M[\mathbf{z}], \lambda_4, \lambda_5, \lambda_6, \lambda_7 \in \mathbb{P}_M^N[\mathbf{z}]}{\text{search}} V_{(k+1)}(\mathbf{z}) \quad (28a)$$

s.t.

$$V_{(k+1)}(\mathbf{z}) - \lambda_4^T \mathbf{G}(\mathbf{z}) - l \in \Sigma_M[\mathbf{z}] \quad (28b)$$

$$-\dot{V}_{(k+1)}(\mathbf{z}) - s_3(1 - V_{(k+1)}(\mathbf{z})) - \bar{s}_4(V_{(k)}(\mathbf{z}) - \gamma) - \lambda_5^T \mathbf{G}(\mathbf{z}) - q_1 \in \Sigma_M[\mathbf{z}] \quad (28c)$$

$$-\bar{s}_5(1 + q_2 - V_{(k)}(\mathbf{z})) + (1 - V_{(k+1)}(\mathbf{z})) - \lambda_6^T \mathbf{G}(\mathbf{z}) \in \Sigma_M[\mathbf{z}] \quad (28d)$$

$$-\bar{s}_6(\gamma - V_{(k)}(\mathbf{z})) + (\gamma - V_{(k+1)}(\mathbf{z})) - \lambda_7^T \mathbf{G}(\mathbf{z}) \in \Sigma_M[\mathbf{z}] \quad (28e)$$

Note that SOSP3 is a linear SOS program and can be solved efficiently with linear SDP techniques. Then,  $D_{(k+1)}(\mathbf{z}) = \{\mathbf{z} \in \mathbb{R}^M | V_{(k+1)}(\mathbf{z}) \leq 1, \mathbf{G}(\mathbf{z}) = \mathbf{0}\}$  is a larger estimated DA.

**Remark 4** From condition (25), we notice that during DA expansion, the derivative of Lyapunov function is required to be negative definite in an annular DA  $\{\mathbf{z} \in \mathbb{R}^M | V_{(k+1)}(\mathbf{z}) \leq 1, V_{(k)}(\mathbf{z}) \geq \gamma, \mathbf{G}(\mathbf{z}) = \mathbf{0}\}$ , not the entire DA  $\{\mathbf{z} \in \mathbb{R}^M | V_{(k+1)}(\mathbf{z}) \leq 1, \mathbf{G}(\mathbf{z}) = \mathbf{0}\}$ . This implies that condition (25b) in the EAD algorithm is more relaxed compared with that in the expanding interior algorithm based on conventional Lyapunov stability theory [31], [32], which facilitates obtaining a tighter estimated DA with less conservativeness.

**Remark 5** The EAD algorithm can provide the estimated DA with an entire boundary for lossy power systems, which contributes to addressing a group of contingencies. Regarding traditional methods, only numerical energy function based on the closest UEP method can estimate an entire DA for lossy power systems. Therefore, we will compare the EAD algorithm with expanding interior algorithm [32] and numerical energy function based on the closest UEP method [42] in Section V to ensure that comparisons are fair.

The flowchart of EAD algorithm for DA estimation is illustrated in Fig. 5, where  $V = [V_1, V_2, \dots, V_{10}]^T$  is the vector for voltage magnitudes of GFM-VSCs; and  $p_0(\mathbf{z})$  and  $\beta_0$  are the known initial values of  $p(\mathbf{z})$  and  $\beta$ , respectively. When SOSP3 is infeasible and  $k > 0$ ,  $D_{(k+1)}(\mathbf{z}) = \{\mathbf{z} \in \mathbb{R}^M | V_{(k+1)}(\mathbf{z}) \leq 1, \mathbf{G}(\mathbf{z}) = \mathbf{0}\}$  is the optimal estimated DA of polynomial system (13). Then, the optimal estimated DA of reduced-order model (11) is obtained with polynomial transformation (12), denoted as  $D_b = \{\mathbf{x} \in \mathbb{R}^N | V(h(\mathbf{x})) \leq 1\}$ .

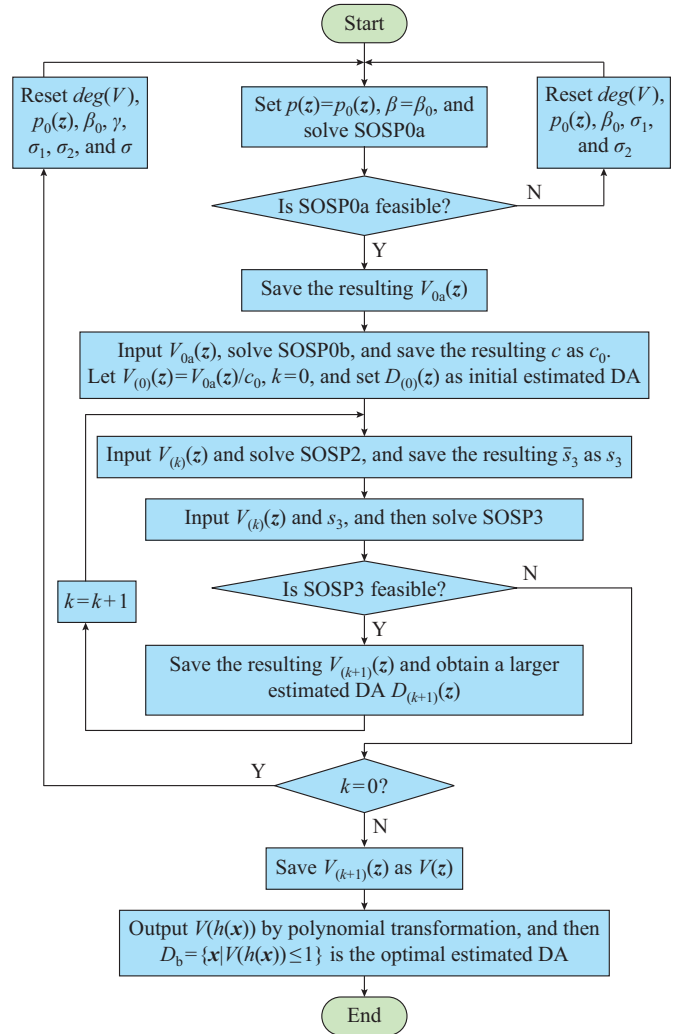


Fig. 5. Flowchart of EAD algorithm for DA estimation.

## V. CASE STUDY

A modified 39-bus system with 10 GFC-VSCs (10-VSC 39-bus system) [13], [38], [39] is presented in Fig. 6. The

parameters of GFM-VSCs are provided in Table I [9], [23], [36], and GFM-VSC 1 is selected as the reference machine with  $\omega_b = 2\pi \times 60$  rad/s and  $S_b = 100$  MVA.

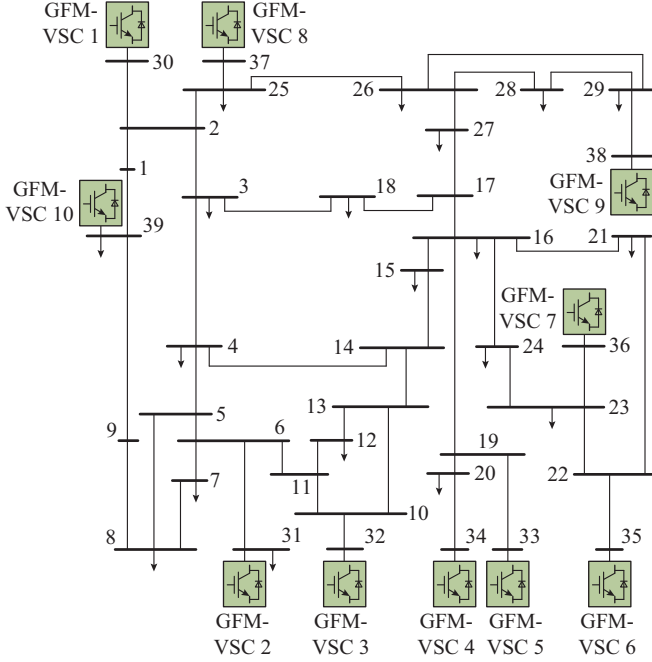


Fig. 6. Layout of a modified 10-VSC 39-bus system.

TABLE I  
PARAMETERS OF GFM-VSCS IN MODIFIED 10-VSC 39-BUS SYSTEM

GFM-VSC	$L_g$ (p.u.)	$L_T$ (p.u.)	$L_{line}$ (p.u.)	$R_{line}$ (p.u.)	$H$ (s)	$K_d$
GFM-VSC 1	0.0060	0.008	0.0101	0.0020	3.00	0.60
GFM-VSC 2	0.0697	0.010	0.0150	0.0026	3.03	0.61
GFM-VSC 3	0.0531	0.010	0.0100	0.0022	3.58	0.72
GFM-VSC 4	0.0436	0.006	0.0082	0.0016	2.86	0.57
GFM-VSC 5	0.1320	0.008	0.0100	0.0020	2.60	0.52
GFM-VSC 6	0.0500	0.004	0.0103	0.0016	3.48	0.70
GFM-VSC 7	0.0490	0.012	0.0152	0.0028	2.64	0.53
GFM-VSC 8	0.0570	0.010	0.0132	0.0025	2.43	0.49
GFM-VSC 9	0.0570	0.006	0.0096	0.0018	3.45	0.69
GFM-VSC 10	0.0110	0.010	0.0100	0.0010	3.20	0.64

By solving the power-flow-like equations, the state variable vector of the reduced-order model at the ASEP is:

$$\mathbf{x}_r = [\theta_{21}, \theta_{31}, \dots, \theta_{(10)1}]^T = [0.0330, 0.3081, 0.3300, 0.5920, 0.3868, 0.4138, 0.3370, 0.5565, -0.0532]^T \quad (29)$$

The vector for voltage magnitudes of GFM-VSCs is:

$$\mathbf{V} = [V_1, V_2, \dots, V_{10}]^T = [1.0558, 1.1210, 1.1426, 1.1052, 1.3275, 1.1676, 1.1067, 1.0755, 1.1481, 1.1397]^T \quad (30)$$

The vector for active power reference of GFM-VSCs is:

$$\mathbf{P}_{ref} = [P_{ref1}, P_{ref2}, \dots, P_{ref10}]^T = [4.00, 2.50, 6.50, 6.32, 5.08, 6.50, 5.60, 5.40, 8.30, 4.86]^T \quad (31)$$

By shifting the ASEP to the origin and performing polynomial transformation (12), we can obtain a transformed state variable vector  $\mathbf{z} = [z_1, z_2, \dots, z_{18}]^T$ . Besides, we set  $\deg(\mathbf{V}) = 2$ ,

$$p_0(\mathbf{z}) = 9 \sum_{i=1}^{18} z_i^2, \quad \beta_0 = 3, \quad \gamma = 0.7, \quad q_1 = q_2 = 10^{-4}, \quad l = l_1 = 10^{-6} \sum_{i=1}^{18} z_i^2, \quad \text{and } l_2 = 10^{-6} \sum_{i=1}^{18} z_i^4 \text{ as the inputs of the EAD algorithm.}$$

#### A. Validity of Reduced-order Model for Multi-VSC Power Systems

To demonstrate the accuracy of reduced-order model for multi-VSC power systems, the exact DAs of reduced-order model and full-order model visualized in the  $\{\theta_{21}, \theta_{31}\}$ ,  $\{\theta_{41}, \theta_{51}\}$ ,  $\{\theta_{61}, \theta_{71}\}$ , and  $\{\theta_{81}, \theta_{91}\}$  planes are illustrated in Fig. 7(a)-(d), respectively. In Fig. 7(a)-(d), the exact DA of reduced-order model is the region surrounded by red dash curve, and that of full-order model is the region surrounded by green solid curve. Note that the precise boundary of exact DA relies on the calculation of all UEPs and their stable manifolds, which is extremely difficult and often inaccurate [31]. To address this issue, the time-domain simulation is used to sample state variables densely in different state planes to depict the rough boundary of exact DA [33], [49].

There are tiny tracking errors between the exact DA of reduced-order model and that of full-order model, which demonstrates that the reduced-order model and full-order model have similar stability characteristics. Hence, we can conclude that the errors between the reduced-order model and full-order model of multi-VSC power systems can be almost ignored, and the estimated DA of the reduced-order model can be regarded as an estimated DA of the full-order model. In this way, the dimension of solution space and computational burden of DA estimation using SOS-based methods can be reduced significantly.

#### B. Transient Stability Analysis of Multi-VSC Power Systems

Next, we illustrate the effectiveness of EAD algorithm. It is noted that the EAD algorithm and expanding interior algorithm are based on reduced-order model (11), while the time-domain simulation and numerical energy function using the closest UEP method are based on full-order model (3).

Figure 8 compares the estimated DAs with the EAD algorithm, expanding interior algorithm [32], and numerical energy function using the closest UEP method [42] with the exact DA. Since it is difficult to portray the exact DA in the three-dimensional space, Fig. 8(a)-(c) merely compares the DAs estimated by the above three methods visualized in the  $\{\theta_{21}, \theta_{31}, \theta_{41}\}$ ,  $\{\theta_{51}, \theta_{61}, \theta_{71}\}$ , and  $\{\theta_{81}, \theta_{91}, \theta_{(10)1}\}$  spaces, respectively. The estimated DAs with the EAD algorithm, expanding interior algorithm, and numerical energy function using the closest UEP method are the regions surrounded by blue outer surface, green inner surface, and yellow inner surface, respectively.

From Fig. 8(a)-(c), we can observe that the EAD algorithm can provide tighter estimated DA than expanding interior algorithm and numerical energy function using the closest UEP method. This is mainly because the expanding interior algorithm requires too many iterative steps based on a more rigorous stability theory, whereas the EAD algorithm is implemented based on the modified Lyapunov stability theory with more relaxed conditions.

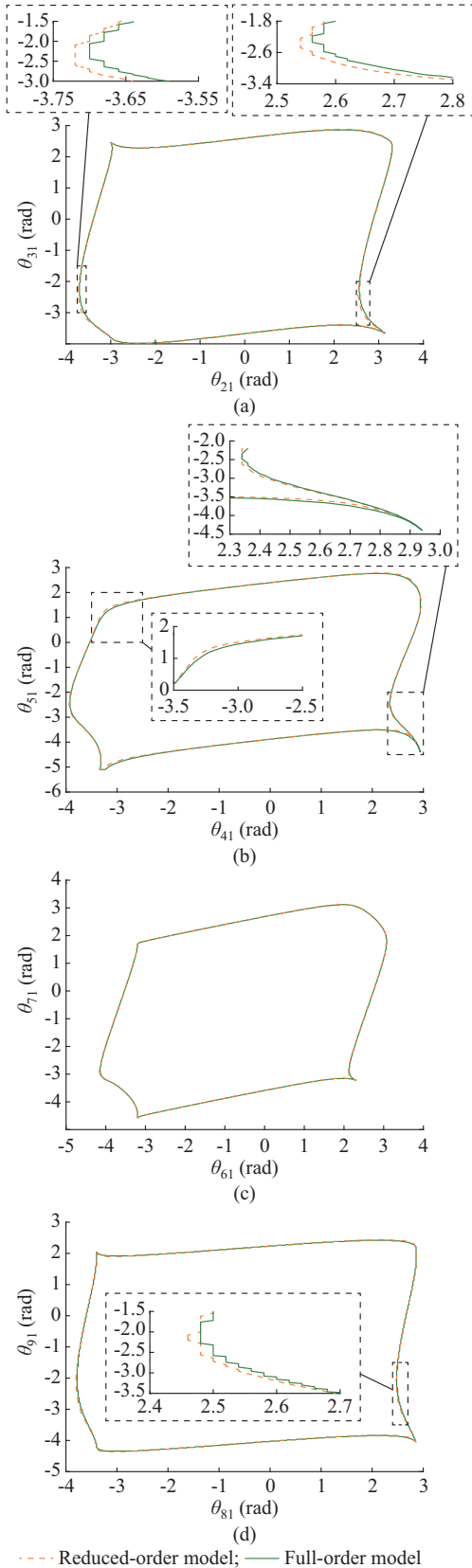


Fig. 7. Exact DAs of full-order model and reduced-order model. (a) In  $\{\theta_{21}, \theta_{31}\}$  plane. (b) In  $\{\theta_{41}, \theta_{51}\}$  plane. (c) In  $\{\theta_{61}, \theta_{71}\}$  plane. (d) In  $\{\theta_{81}, \theta_{91}\}$  plane.

Moreover, numerical energy function using the closest UEP method provides the most conservative estimated re-

sults. In conclusion, the EAD algorithm can provide much tighter estimated DA than existing methods.

To further demonstrate the accuracy of EAD algorithm, the estimated DAs and exact DA visualized in  $\{\theta_{21}, \theta_{31}\}$ ,  $\{\theta_{61}, \theta_{71}\}$ , and  $\{\theta_{81}, \theta_{91}\}$  planes are compared in Fig. 8(d)-(f), respectively. The DAs estimated by the EAD algorithm, expanding interior algorithm, and numerical energy function using the closest UEP method are the regions surrounded by red solid curve, blue solid curve, and magenta solid curve, respectively.

The rough exact DA of full-order model is the region surrounded by green solid curve, which is obtained from Fig. 7(a), (c), and (d).

It is shown that the EAD algorithm can also provide better estimated DA than expanding interior algorithm and numerical energy function using the closest UEP method, which is consistent with the results in Fig. 8(a)-(c). Besides, the EAD algorithm will not give the optimistic estimated results.

Note that local methods such as boundary of stability region based controlling unstable equilibrium point (CUEP) method may give more accurate estimates than the EAD algorithm under some faults, but they depend on a specific fault and cannot address a group of contingencies. However, the EAD algorithm can provide the estimated DA with an entire boundary. This means that the estimated DA with the EAD algorithm is independent of specific faults and has the potential to deal with a group of contingencies. As long as the initial state of post-fault system (the fault-cleared state) is in the estimated DA, the post-fault dynamics are stable, and the computation of the entire post-fault trajectory is not required. This feature can reduce computational costs on similar dynamics of post-fault systems dramatically.

To further illustrate the accuracy of EAD algorithm, Table II compares the exact critical clearing time (CCT) using time-domain simulation and estimated CCT using the above three methods, where a three-phase-to-ground fault occurs on different buses shown in Table II at  $t=0.1$  s.

Since exploiting fault-on trajectories can reduce the conservativeness of estimated CCT, we check each state along the fault-on dynamics until the value of Lyapunov function  $V(\mathbf{x})$  at a state  $x(t_c)$  reaches the maximum estimated critical value, then the corresponding time  $t_c$  is the estimated CCT [50].

As shown in Table II, the EAD algorithm enhances the accuracy of estimated CCT by about 16.71%, and 48.09% on average compared with those with expanding interior algorithm and numerical energy function using the closest UEP method, respectively.

Such improvement mainly stems from the modified Lyapunov stability theory with less strict conditions. Among all the buses in column 1 of Table II, the estimated CCT for buses  $\{6, 31, 35, 39\}$  has a high accuracy of over 95%.

Note that the estimated CCT for bus 39 has the highest accuracy of 99.29%, whereas the estimated CCT for bus 2 has the lowest accuracy of 38.75%, and the average accuracy is about 79.02%. These results show the effectiveness of EAD algorithm.

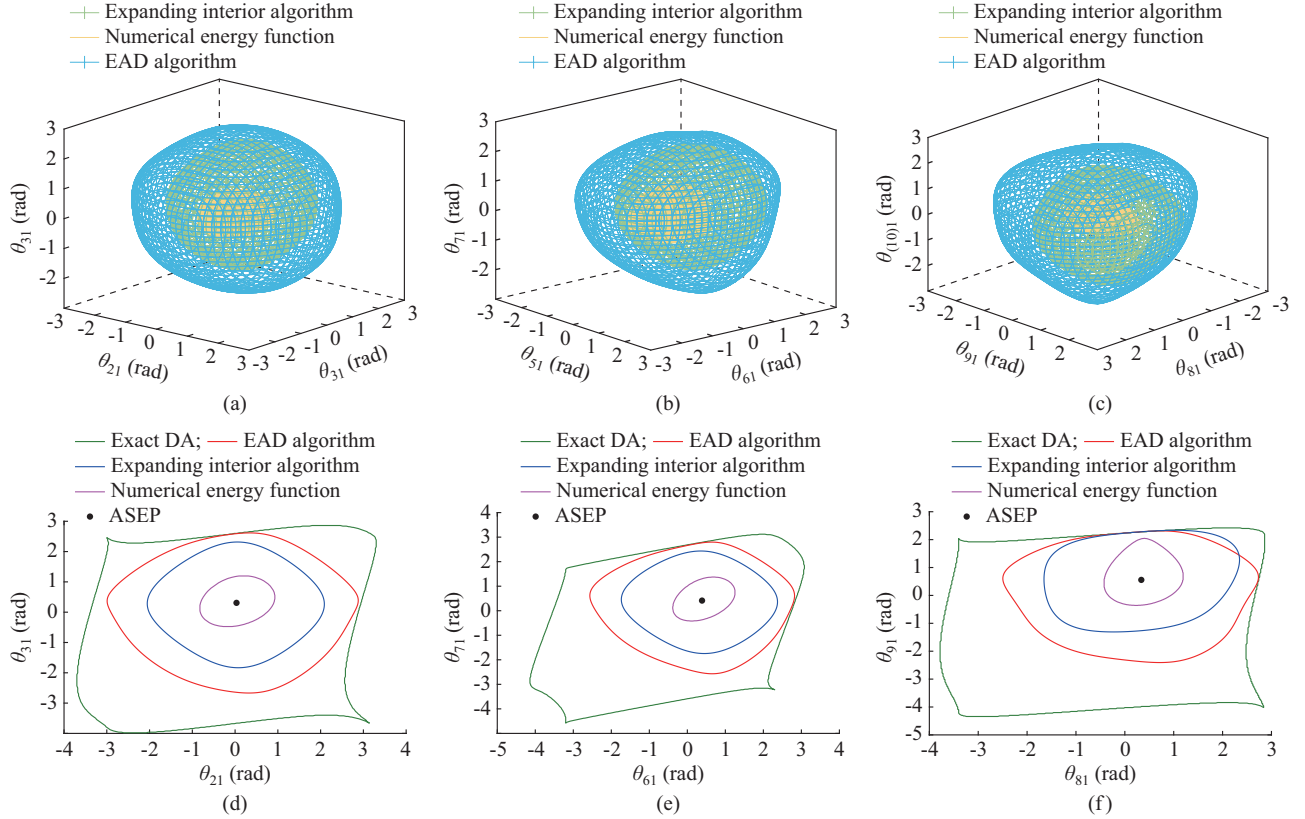


Fig. 8. Estimated DA with different methods and exact DA. (a) In  $\{\theta_{21}, \theta_{31}, \theta_{41}\}$  space. (b) In  $\{\theta_{51}, \theta_{61}, \theta_{71}\}$  space. (c) In  $\{\theta_{81}, \theta_{91}, \theta_{101}\}$  space. (d) In  $\{\theta_{21}, \theta_{31}\}$  plane. (e) In  $\{\theta_{61}, \theta_{71}\}$  plane. (f) In  $\{\theta_{81}, \theta_{91}\}$  plane.

TABLE II  
COMPARISONS OF EXACT CCT UNDER THREE-PHASE-TO-GROUND FAULT OF MODIFIED 10-VSC 39-BUS SYSTEM

Bus	CCT (s)			
	Numerical energy function	Expanding interior algorithm	EAD algorithm	Time-domain simulation
2	0.123	0.202	0.235	0.607
6	0.333	0.964	1.128	1.139
16	0.138	0.218	0.282	0.521
19	0.125	0.201	0.236	0.317
21	0.192	0.336	0.465	0.717
23	0.148	0.256	0.326	0.414
31	0.476	1.035	1.427	1.470
33	0.109	0.216	0.260	0.300
35	0.132	0.271	0.347	0.357
39	0.161	0.453	0.614	0.618

C. Influence of Parameters on Transient Stability

According to Remark 3, to ensure the accuracy of the reduced-order model for multi-VSC power systems, parameters  $H$  and  $K_d$  of GFM-VSC need to meet conditions  $2H \ll \omega_b$  and  $K_d \gg 2H/\omega_b$ .

To quantitatively provide the conditions of using singular perturbation theory, we compare the exact DAs of reduced-order model and full-order model when parameters  $H$  and  $K_d$  vary. Figure 9(a)-(f) visualizes the exact DAs of full-order

model and reduced-order model when parameters  $H$  and  $K_d$  vary in the  $\{\theta_{81}, \theta_{91}\}$  plane. Note that initial parameters  $H_0$  and  $K_{d0}$  take the values in columns 6 and 7 of Table I, respectively.

From Fig. 9, it is observed that as the equivalent inertial coefficient increases, the difference between the reduced-order model and full-order model also gradually rises. When the inertia emulation coefficient increases to  $[15H_0, 25H_0]$  that is approximately equal to the inertia coefficient of SG, the gap between reduced-order model and full-order model is huge and cannot be ignored. In this case, the reduced-order modeling method based on singular perturbation theory will introduce large errors and is no longer suitable. Similarly, when the damping coefficient  $K_{d0}$  decreases below  $K_{d0}/5$ , the reduced-order modeling method will bring large errors as well.

In summary, when  $K_d > K_{d0}/5$  and  $H < 5H_0$  hold, the accuracy of reduced-order modeling method based on singular perturbation theory can be guaranteed.

VI. CONCLUSION

This paper uses singular perturbation theory to derive the reduced-order model of multi-VSC power systems and presents an EAD algorithm to estimate the DA with an entire boundary. The main conclusions are as follows.

- 1) The exact DA of reduced-order model presents a nearly error-free approximation for that of full-order model when parameters  $H$  and  $K_d$  of GFM-VSC satisfy the conditions  $2H \ll \omega_b$ ,  $K_d \gg 2H/\omega_b$ , respectively.

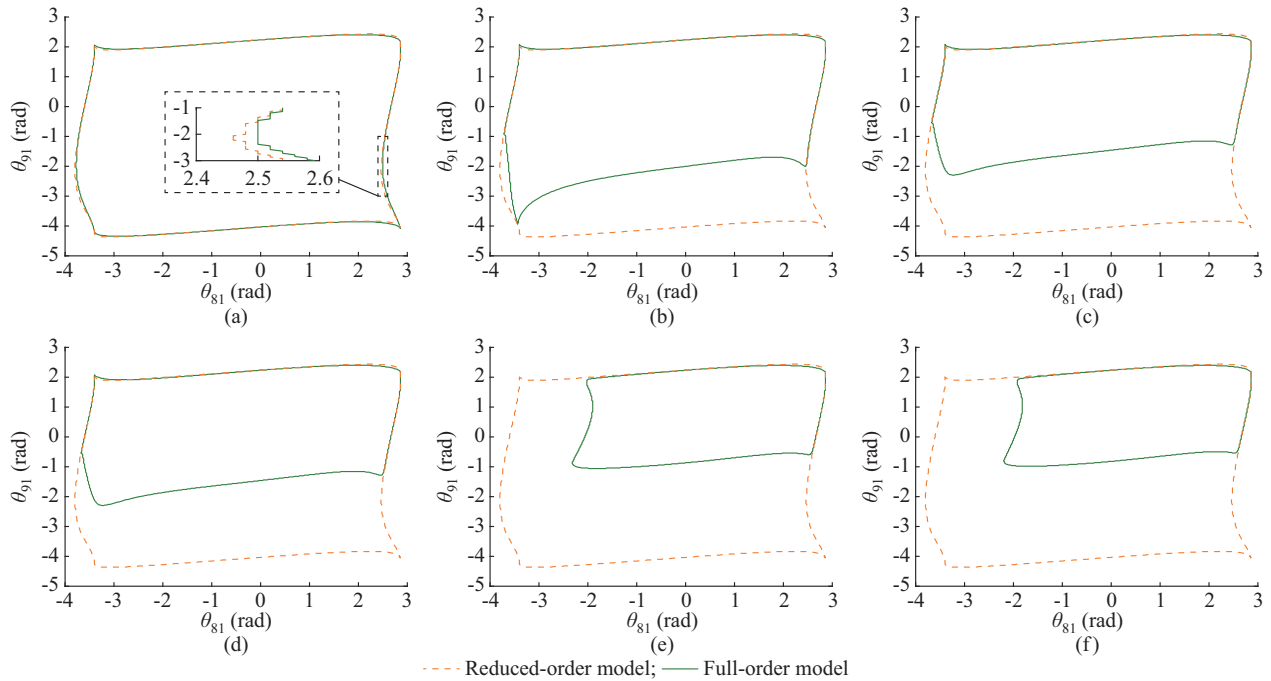


Fig. 9. Exact DAs of full-order model and reduced-order model when parameters  $H$  and  $K_d$  vary in  $\{\theta_{81}, \theta_{91}\}$  plane. (a)  $H=5H_0$  and  $K_d=K_{d0}$ . (b)  $H=15H_0$  and  $K_d=K_{d0}$ . (c)  $H=25H_0$  and  $K_d=K_{d0}$ . (d)  $H=H_0$  and  $K_d=K_{d0}/5$ . (e)  $H=H_0$  and  $K_d=K_{d0}/10$ . (f)  $H=5H_0$  and  $K_d=K_{d0}/5$ .

2) Compared with existing global DA estimation methods such as expanding interior algorithm and numerical energy function using the closest UEP method, the EAD algorithm can provide much better estimated DA and CCT. The highest accuracy of estimated CCT can reach 99.29%.

In the future, the following directions will be explored.

1) A more detailed model of multi-VSC power systems considering the dynamics of VCL, CCL, and  $Q$ - $V$  loop.

2) Robust DA estimation considering uncertain parameters, including uncertain active power reference, uncertain susceptance, and conductance of multi-VSC power systems.

## REFERENCES

- [1] F. Blaabjerg, R. Teodorescu, M. Liserre *et al.*, "Overview of control and grid synchronization for distributed power generation systems," *IEEE Transactions on Industrial Electronics*, vol. 53, no. 5, pp. 1398-1409, Oct. 2006.
- [2] Q. H. Wu, A. Bose, C. Singh *et al.*, "Control and stability of large-scale power system with highly distributed renewable energy generation: viewpoints from six aspects," *CSEE Journal of Power and Energy Systems*, vol. 9, no. 1, pp. 8-14, Jan. 2023.
- [3] Q. H. Wu, Y. Lin, C. Hong *et al.*, "Transient stability analysis of large-scale power systems: a survey," *CSEE Journal of Power and Energy Systems*, vol. 9, no. 4, pp. 1284-1300, Jul. 2023.
- [4] X. Fu, J. Sun, M. Huang *et al.*, "Large-signal stability of grid-forming and grid-following controls in voltage source converter: a comparative study," *IEEE Transactions on Power Electronics*, vol. 36, no. 7, pp. 7832-7840, Jul. 2021.
- [5] B. K. Poolla, D. Groß, and F. Dörfler, "Placement and implementation of grid-forming and grid-following virtual inertia and fast frequency response," *IEEE Transactions on Power Systems*, vol. 34, no. 4, pp. 3035-3046, Jul. 2019.
- [6] A. Tayyebi, D. Groß, A. Anta *et al.*, "Frequency stability of synchronous machines and grid-forming power converters," *IEEE Journal of Emerging and Selected Topics in Power Electronics*, vol. 8, no. 2, pp. 1004-1018, Jun. 2020.
- [7] J. Rocabert, A. Luna, F. Blaabjerg *et al.*, "Control of power converters in AC microgrids," *IEEE Transactions on Power Electronics*, vol. 27, no. 11, pp. 4734-4749, Nov. 2012.
- [8] C. Arghir, T. Jouini, and F. Dörfler, "Grid-forming control for power converters based on matching of synchronous machines," *Automatica*, vol. 95, pp. 273-282, Sept. 2018.
- [9] C. Yang, L. Huang, H. Xin *et al.*, "Placing grid-forming converters to enhance small signal stability of PLL-integrated power systems," *IEEE Transactions on Power Systems*, vol. 36, no. 4, pp. 3563-3573, Jul. 2021.
- [10] J. Yu, Y. Qi, H. Deng *et al.*, "Evaluating small-signal synchronization stability of grid-forming converter: a geometrical approach," *IEEE Transactions on Industrial Electronics*, vol. 69, no. 9, pp. 9087-9098, Sept. 2022.
- [11] S. Eberlein and K. Rudion, "Impact of inner control loops on small-signal stability and model-order reduction of grid-forming converters," *IEEE Transactions on Smart Grid*, vol. 14, no. 4, pp. 2812-2824, Jul. 2023.
- [12] L. Zhao, Z. Jin, and X. Wang, "Small-signal synchronization stability of grid-forming converters with regulated DC-link dynamics," *IEEE Transactions on Industrial Electronics*, vol. 70, no. 12, pp. 12399-12409, Jan. 2023.
- [13] Z. Yang, M. Zhan, D. Liu *et al.*, "Small-signal synchronous stability of a new-generation power system with 100% renewable energy," *IEEE Transactions on Power Systems*, vol. 38, no. 5, pp. 4269-4280, Oct. 2022.
- [14] T. Liu and X. Wang, "Transient stability of single-loop voltage-magnitude controlled grid-forming converters," *IEEE Transactions on Power Electronics*, vol. 36, no. 6, pp. 6158-6162, Jun. 2021.
- [15] M. Chen, D. Zhou, and F. Blaabjerg, "Enhanced transient angle stability control of grid-forming converter based on virtual synchronous generator," *IEEE Transactions on Industrial Electronics*, vol. 69, no. 9, pp. 9133-9144, Sept. 2022.
- [16] N. Hatziaargyriou, J. Milanovic, C. Rahmann *et al.*, "Definition and classification of power system stability – revisited & extended," *IEEE Transactions on Power Systems*, vol. 36, no. 4, pp. 3271-3281, Jul. 2021.
- [17] L. Huang, H. Xin, Z. Wang *et al.*, "Transient stability analysis and control design of droop-controlled voltage source converters considering current limitation," *IEEE Transactions on Smart Grid*, vol. 10, no. 1, pp. 578-591, Sept. 2017.
- [18] Y. Li, Y. Gu, and T. C. Green, "Revisiting grid-forming and grid-following inverters: a duality theory," *IEEE Transactions on Power Systems*, vol. 37, no. 6, pp. 4541-4554, Nov. 2022.
- [19] H. D. Chiang, *Direct Methods for Stability Analysis of Electric Power Systems: Theoretical Foundation, BCU Methodologies, and Applications*. Hoboken: John Wiley & Sons, 2011.

- [20] D. Han, A. El-Guindy, and M. Althoff, "Estimating the domain of attraction based on the invariance principle," in *Proceedings of 2016 IEEE 55th Conference on Decision and Control*, Las Vegas, USA, Dec. 2016, pp. 5569-5576.
- [21] Y. Tang, Z. Tian, X. Zha *et al.*, "An improved equal area criterion for transient stability analysis of converter-based microgrid considering nonlinear damping effect," *IEEE Transactions on Power Electronics*, vol. 37, no. 9, pp. 11272-11284, Sept. 2022.
- [22] H. Xiao, H. He, L. Zhang *et al.*, "Adaptive grid-synchronization based grid-forming control for voltage source converters," *IEEE Transactions on Power Systems*, vol. 39, no. 2, pp. 4763-4766, Mar. 2024.
- [23] J. Lei, X. Xiang, Q. Qu *et al.*, "On the destabilizing mechanism of nonuniform damping in grid-forming converters penetrated multi-machine system," *IEEE Transactions on Power Systems*, vol. 39, no. 3, pp. 5435-5438, May 2024.
- [24] Z. Tian, X. Li, X. Zha *et al.*, "Transient synchronization stability of an islanded AC microgrid considering interactions between grid-forming and grid-following converters," *IEEE Journal of Emerging and Selected Topics in Power Electronics*, vol. 11, no. 4, pp. 4463-4476, Apr. 2023.
- [25] Z. Shuai, C. Shen, X. Liu *et al.*, "Transient angle stability of virtual synchronous generators using Lyapunov's direct method," *IEEE Transactions on Smart Grid*, vol. 10, no. 4, pp. 4648-4661, Jul. 2019.
- [26] G. Chesi, *Domain of Attraction: Analysis and Control via SOS Programming*. New York: Springer, 2011.
- [27] C. Mishra, A. Pal, J. S. Thorp *et al.*, "Transient stability assessment of prone-to-trip renewable generation rich power systems using Lyapunov's direct method," *IEEE Transactions on Sustainable Energy*, vol. 10, no. 3, pp. 1523-1533, Jul. 2019.
- [28] X. Li, Z. Wang, Y. Liu *et al.*, "The largest estimated domain of attraction and its applications for transient stability analysis of PLL synchronization in weak-grid-connected VSCs," *IEEE Transactions on Power Systems*, vol. 38, no. 5, pp. 4107-4121, Sept. 2023.
- [29] Z. Zhang, R. Schuerhuber, L. Fickert *et al.*, "Domain of attraction's estimation for grid connected converters with phase-locked loop," *IEEE Transactions on Power Systems*, vol. 37, no. 2, pp. 1351-1362, Mar. 2022.
- [30] C. Zhang, M. Molinas, Z. Li *et al.*, "Synchronizing stability analysis and region of attraction estimation of grid-feeding VSCs using sum-of-squares programming," *Frontiers in Energy Research*, vol. 8, p. 56, Apr. 2020.
- [31] M. Anghel, F. Milano, and A. Papachristodoulou, "Algorithmic construction of Lyapunov functions for power system stability analysis," *IEEE Transactions on Circuits and Systems I: Regular Papers*, vol. 60, no. 9, pp. 2533-2546, Sept. 2013.
- [32] S. Izumi, H. Somekawa, X. Xin *et al.*, "Analysis of robust transient stability of power systems using sum of squares programming," *International Journal of Electrical Power & Energy Systems*, vol. 115, p. 105401, Feb. 2020.
- [33] Y. Lin, T. Wen, Y. Liu *et al.*, "Expanding annular domain algorithm to estimate domains of attraction for power system stability analysis," *CSEE Journal of Power and Energy Systems*, vol. 10, no. 5, pp. 1925-1934, Sept. 2024.
- [34] M. G. Taul, X. Wang, P. Davari *et al.*, "Reduced-order and aggregated modeling of large-signal synchronization stability for multiconverter systems," *IEEE Journal of Emerging and Selected Topics in Power Electronics*, vol. 9, no. 3, pp. 3150-3165, Aug. 2020.
- [35] D. Pal and B. K. Panigrahi, "Reduced-order modeling and transient synchronization stability analysis of multiple heterogeneous grid-tied inverters," *IEEE Transactions on Power Delivery*, vol. 38, no. 2, pp. 1074-1085, Apr. 2023.
- [36] M. Ebrahimi, S. A. Khajehoddin, and M. Karimi-Ghartemani, "An improved damping method for virtual synchronous machines," *IEEE Transactions on Sustainable Energy*, vol. 10, no. 3, pp. 1491-1500, Feb. 2019.
- [37] M. Zhao, X. Yuan, J. Hu *et al.*, "Voltage dynamics of current control time-scale in a VSC-connected weak grid," *IEEE Transactions on Power Systems*, vol. 31, no. 4, pp. 2925-2937, Jul. 2016.
- [38] K. Strunz, K. Almunem, C. Wulkow *et al.*, "Enabling 100% renewable power systems through power electronic grid-forming converter and control: system integration for security, stability, and application to Europe," *Proceedings of the IEEE*, vol. 111, no. 7, pp. 891-915, Jul. 2023.
- [39] J. Y. Park and J. W. Chang, "Novel autonomous control of grid-forming DGs to realize 100% renewable energy grids," *IEEE Transactions on Smart Grid*, vol. 15, no. 3, pp. 2866-2880, May 2024.
- [40] G. Peponides, P. Kokotovic, and J. Chow, "Singular perturbations and time scales in nonlinear models of power systems," *IEEE Transactions on Circuits and Systems*, vol. 29, no. 11, pp. 758-767, Nov. 1982.
- [41] M. Pai, *Energy Function Analysis for Power System Stability*. Berlin: Springer Science & Business Media, 1989.
- [42] H. Didier and G. Andrea, *Positive Polynomials in Control*. Berlin: Springer, 2005.
- [43] P. A. Parrilo, *Structured Semidefinite Programs and Semialgebraic Geometry Methods in Robustness and Optimization*. Pasadena: California Institute of Technology, 2000.
- [44] J. Lofberg, "YALMIP: a toolbox for modeling and optimization in MATLAB," in *Proceedings of 2004 IEEE International Conference on Robotics and Automation*, Taipei, China, Sept. 2004, pp. 284-289.
- [45] M. ApS. (2009, Dec.). MOSEK optimization toolbox for MATLAB. [Online]. Available: <https://docs.mosek.com/latest/toolbox/index.html>.
- [46] L. Chen, T. Wen, Y. Lin *et al.*, "Improved EAD algorithm to estimate domains of attraction of power systems including induction motors for transient voltage stability analysis," *CSEE Journal of Power and Energy Systems*, vol. 10, no. 6, pp. 2321-2332, Nov. 2024.
- [47] S. Wang, Z. She, and S. Ge, "Estimating minimal domains of attraction for uncertain nonlinear systems," *IEEE Transactions on Systems, Man, and Cybernetics: Systems*, vol. 51, no. 12, pp. 7776-7787, Dec. 2021.
- [48] J. Liu, Y. Zhang, A. J. Conejo *et al.*, "Ensuring transient stability with guaranteed region of attraction in DC microgrids," *IEEE Transactions on Power Systems*, vol. 38, no. 1, pp. 681-691, Jan. 2023.
- [49] L. Chen, T. Wen, Y. Lin *et al.*, "Two-stage expanding boundary algorithm to estimate domains of attraction of large-scale power systems with induction motors," *IEEE Transactions on Power Systems*, vol. 40, no. 1, pp. 1010-1023, Jan. 2025.

**Lei Chen** received the M.S. degree from Changsha University of Science and Technology, Changsha, China, in 2021, and the Ph.D. degree from South China University of Technology, Guangzhou, China, in 2025. He is currently working in the Electric Power Research Institute, China Southern Power Grid, Guangzhou, China. His research interests include power system transient stability analysis, planning, and operation.

**Tianhao Wen** received the B.S. degree from Huazhong University of Science and Technology, Wuhan, China, in 2018, and the Ph.D. degree from South China University of Technology, Guangzhou, China, in 2023. He is currently a Postdoctoral Researcher with the School of Electric Power Engineering, South China University of Technology. His research interests include nonlinear observer and power system transient stability analysis.

**Yuqing Lin** received the B.S. and Ph.D. degrees from South China University of Technology, Guangzhou, China, in 2019 and 2024, respectively. He is currently a Postdoctoral Researcher with the School of Electric Power Engineering, South China University of Technology. His research interests include power system transient stability analysis and control of wind power generation system.

**Yang Liu** received the B.E. and Ph.D. degrees from South China University of Technology, Guangzhou, China, in 2012 and 2017, respectively. He is currently an Associate Professor with the School of Electric Power Engineering, South China University of Technology. His research interests include power system stability analysis and control, control of wind power generation system, and nonlinear control theory.

**Yingjie Qin** received the Ph.D. degree from South China University of Technology, Guangzhou, China, in 2021. She is currently working in the Power Dispatching and Control Center, Guangdong Power Grid Corporation, Guangzhou, China. Her research interests include power system operation and transient stability analysis.

**Qing-Hua Wu** received the M.S. degree from Huazhong University of Science and Technology, Wuhan, China, in 1981, and the Ph.D. degree from the Queen's University of Belfast (QUB), Belfast, U.K., in 1987. He worked as the Chair Professor in Liverpool University, Liverpool, U.K., from 1995 to 2012. He is currently a Distinguished Professor and the Director of Energy Research Institute, South China University of Technology, Guangzhou, China. He is a Life Fellow of IEEE, Fellow of IET, Fellow of CSEE, Fellow of AAIA, and Chartered Engineer. His research interests include nonlinear adaptive control, mathematical morphology, artificial intelligence, and power system operation and control.